International Journal of Recent Technology and Engineering (IJRTE)
ISSN: 2277-3878 (Online), Volume-10 Issue-4, November 2021

Experimental Validating DC Motor Models and Identify Transfer Function

Meshari J. Al Jandal, Khaled S. Al Rasheed, Muhammad R. Jamal

Abstract: ***DC Motor is an essential element for many applications in the field of automation, robotics, and many others. They are important for many engineers to understand its behaviours and characteristics. However, controlling any system is still a challenge because of their abnormal behavior. In this paper, we are applying techniques to understand the behavior of servo system. Several groups of researchers conducted experiments based on a standard first-order model of a DC Motor using first principles modeling to derive the parameters. However, not much highlighting is identified on how well these models match up the actual data. In this paper, a deeper understanding has been taken place to gain some familiarity in testing and measurements by exploring a special arrangement in a laboratory called Quanser QUBE-Servo. In addition to this, signals monitoring on the live-mode has the advantage of gaining conceptual knowledge in the experimental test, analysis, and verification of the system. On the other hand, solving differential equations numerically using powerful software such as LabVIEW which endorses the comprehension of the system operation. In general, this report discusses a simple technique to study the DC motor transient response, read the angular position of the encoder by interface data acquisition device used with LabVIEW software.***

Keywords: DC Motor; stability; Low-pass filter; Quanser QUBE-Servo; close-loop control; incremental encoder; FBGA; cutoff frequency; LabVIEW

I. INTRODUCTION

A. System Description

The QUBE-Servo pictured in Figure1-1 is a solidify aluminum box frame equipped internally with a permanent magnet DC motor coupled to an encoder to measure the angular position. The QUBE-Servo connected to digital controller based on field-programmable gate array (FBGA) input/output interfaces called myRIO. The QUBE-Servo include built-in amplifier command and encoder port to interface with an external data acquisition directly through the port using ribbon cable. The communication between the QUBE-Servo systems with the controller peripherals is illustrated in Figure1-2.

Manuscript received on October 07, 2021.
Revised Manuscript received on October 11, 2021.
Manuscript published on October 30, 2021.
* Correspondence Author
Meshari J Al Jandal, Department of Electrical Engineering from Kuwait University, located in Kuwait
Khaled S Al Rasheed, Department of Electrical and Electronics Engineering from New Mexico State University located in Kuwait
Muhammad R A A Jamal*, Member of Training Staff, Higher Institute of Energy PAAET, Kuwait

Figure 1-1: Quanser QUBE-Servo interact with my RIO (FBGA base) via LabVIEW.

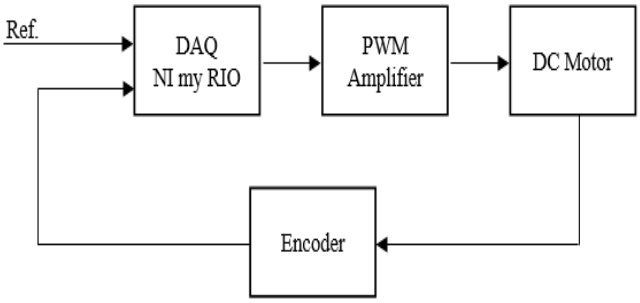

Figure 1-2: Block Diagram of QUBE-Servo system.

The analogue output of the controller is connected to the power PWM amplifier in which the motor driver received the command signal to operate. The incremental encoder coupled mechanically with the DC motor shaft in such a way the encoder generates a signal proportional to the angular rotation in order to allocate the rate change of angular velocity. The controller is linked to the personal computer PC through the USB port to create a virtual graphical user interface GUI to interact physically with the system of the QUBE-Servo. LabVIEW is used to drive the DC motor and read the encoder signal that represents the angular position of the disc.

B. System Modeling

DC Motor

The QUBE-servo integrates an Allied Motion CL40 Series Coreless DC Motor model 16705. This is a high-performance permanent magnet, no cogging, no iron loss, and low inertia rotor for the rapid response due to small inductance. Consequently, it can obtain a faster response behavior compared to the conventional DC motor.

The DC motor can be modeled as shown in the schematic of the equivalent representation of DC motor in Figure 1-4. The electromechanical parameters are given in table 1-2 (The below table taken from first principles modeling manual [5]).

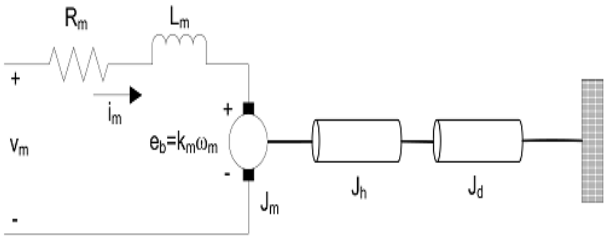

Figure 1-3: QUBE-Servo DC motor and load

The DC motor transfer function will be modeled for a linear approximation with neglecting the second order effects such as hysteresis and voltage drop across brushes [6]. The air gap flux ϕ is constant over the time which developed from the permanent magnet placed on the inner side of the cylindrical stator. So, the back electromotive force eb is linearly propositional to the angular velocity ωm multiply by constant km, which is known as Motor back-emf constant, as follows:

$$e_b = k_m \omega_m \quad (1)$$

The output torque is linearly proportional to the armature current im by the constant kt , which is known as Torque constant as follows:

$$T = k_t i_m \quad (2)$$

The DC motor shaft is coupled to the load hub which is a solid metal disk used to hold the disk that has a moment of inertia of Jh. A disk load is linked to the output shaft with a moment of inertia of Jd. The physical quantities of electrical and mechanical parameters are given in table 1-2 (The below table taken from first principles modeling manual [5]).

Table 1: QUBE-Servo system parameters

Symbol	Description	Value
DC Motor		
R_m	Terminal resistance	8.4Ω
k_t	Torque constant	0.042 N.m/A
k_m	Motor back-emf constant	0.042 V/(rad/s)
J_m	Rotor inertia	4.0×10^{-6} kg.m^2
L_m	Rotor inductance	1.16 mH
Load Hub		
m_h	Load hub mass	0.0106 kg
r_h	Load hub radius	0.0111 m
Load Disk		
m_d	Load disk mass	0.053 kg
r_d	Load disk radius	0.0248 m

Apply the kirchoff's voltage law:

$$-v_m + R_m i_m + L_m \frac{di_m}{dt} + e_b = 0 \quad (3)$$

Since the inductance Lm is very small compared to resistance, it can be ignored. Then, the equation becomes:

$$-v_m + R_m i_m + e_b = 0 \quad (4)$$

The second law of Newton's with considering zero friction can be driven as the following equations:

$$J_{eq} \frac{d\omega_m}{dt} = T \quad (5)$$

Where Jeq=Jd+Jh, is the total moment of inertia stand-in on the motor shaft. The moment of inertia (J) of a disk about its pivot point, with mass m and radius r can be calculated as follow:

$$J = \frac{1}{2} m r^2 \quad (6)$$

Next, taking the Laplace transform of [4] and [5], which can be written as:

$$v_{m(s)} = +R_m I_{m(s)} + k_m I_{m(s)} \quad (7)$$

$$J_{eq}\, S\, \omega_{m(s)} = k_t I_{m(s)} \quad (8)$$

Then, after applying some algebraic manipulation, where k = kt = km using the SI unit's assumption to obtain:

$$\frac{\omega_{m(s)}}{V_{m(s)}} = \frac{\frac{1}{k}}{\frac{R_m J_{eq}}{k^2} s + 1} \quad (9)$$

Where $K = \frac{1}{k}$ and $\tau = \frac{R_m J_{eq}}{k^2}$

Finally, The QUBE-Servo voltage-to-speed transfer function of QUBE-servo system is

$$\frac{\omega_{m(s)}}{V_{m(s)}} = \frac{K}{\tau s + 1} \quad (10)$$

C. Motor Encoder

The technology of optical sensing encoder has been proven its capability in the control system. This type knows as an incremental encoder which is the most widely used due to its low cost and capability to provide signal information related to the system [7]. The encoder associated with QUBE-Servo is a single-ended optical shaft. It can generate serial pulses of 512 in one revolution. It can provide information by shaping tow square wave cycles output of 90 degrees out of phase that often called quadrant_signals, as illustrated in Figure 1-5: *[7]*

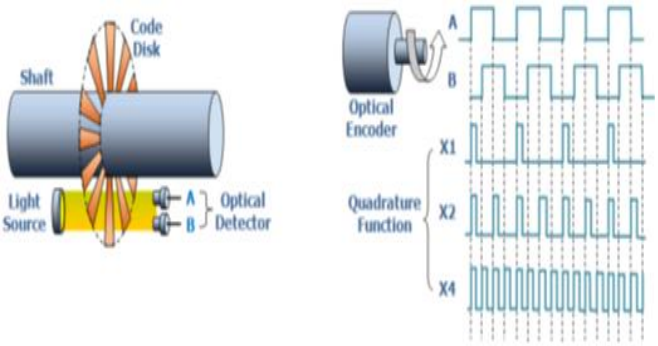

Figure 1-4: working principle of incremental optical encoder

The above Figure 1-6 shows how incremental optical encoder signal produce two channels which can be used to provide more resolution by calculating both Lead/Lag edges of both channels which eventually quadruple the number of pulses (4x512=2048 pulses) [8].

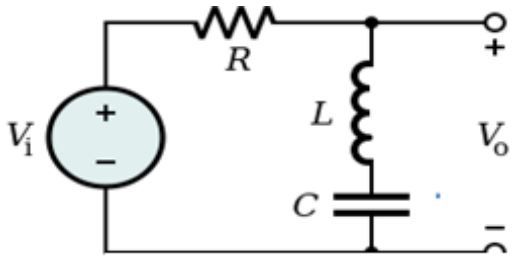

Figure 1-5: Lowpass filter

D. Filtering

The rapid advancement in technology to develop a permanent magnet DC motor for high-speed application is widely used in the industrial sector for maximum efficiency [9]. There are several research has become an important topic to explore in the way of measuring the position of the DC motor. There are different methods to sense the rotor position of the DC motor such as the back electromotive force (back EMF) method [10]. The main intention for this method to obtain precise estimates of the rotor speed and the signal produced from the EMF. As a result of this, several techniques have been proposed to provide the best result of EMF by apply low pass filter [11], as shown in Figure 1-7 to clear the high-frequency noise. The low pass filter is an electronic circuit based on passive components that passes signals with a lower frequency and [12]. The first order low-pass with cutoff frequency has a transfer function of the form:

$$G(s = j\omega) = \frac{\frac{1}{\tau}}{s + \frac{1}{\tau}} = \frac{1}{j\omega * \tau + 1}$$

$G(s) = \frac{\omega_f}{s+\omega_f}$; Where ω_f is the cutoff frequency of the filter in radians per seconds (rad/s)

II. RESULTS & DISCUSSIONS

A. Creating a LabVIEW VI

In this section, several steps have been done according to the workbook manual procedures in order to build a simple LabVIEW virtual interface VI to communicate with QUBE-servo using QRCPT driver as follows:

- Run the LabVIEW software and create a new VI starting with the Quanser Basic Hardware Loop template as shown in Figure 1-10.

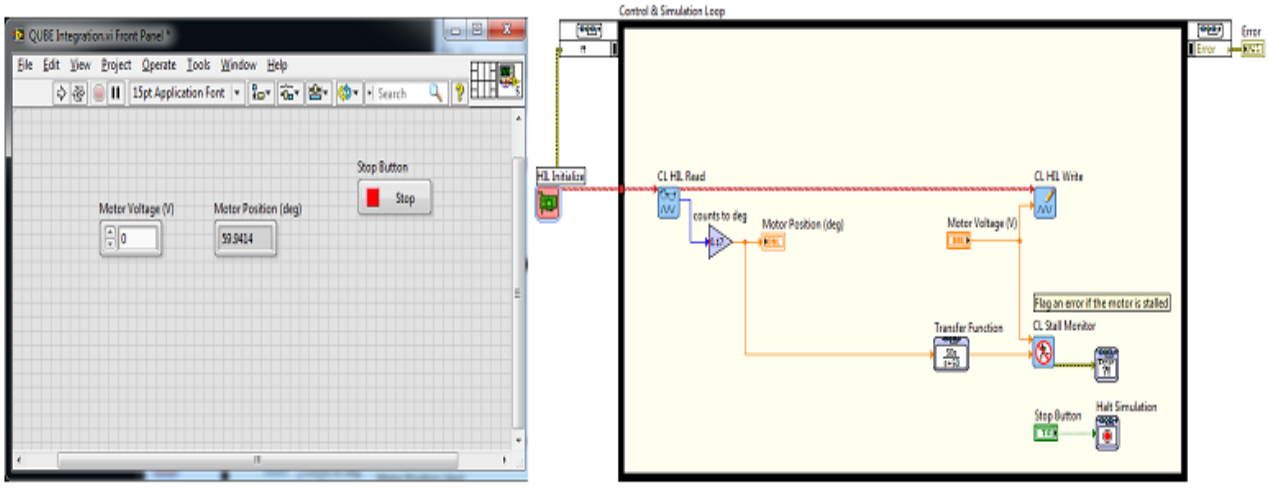

Figure 1-6: VI used with QRCPT to drive motor and read angle on QUBE-Servo, where left side screen represent the front panel and the other side is the block diagram.

- The simulation parameters can be configured on the simulation loop input node by double click on the border of the block diagram to access the simulation parameters as shown in Figure 1-11.
- Then, simulation parameters and timing parameters were configured as the following table 1-3:

Simulation parameters		Timing parameters	
Final time (s)	Inf	Select	Synchronize Loop to Timing Source
ODE Solver	Runge-Kutta 1 (Euler)	Timing Source	1 kHz Clock
Step Size (s)	0.002 (500Hz)	Select	Auto Period

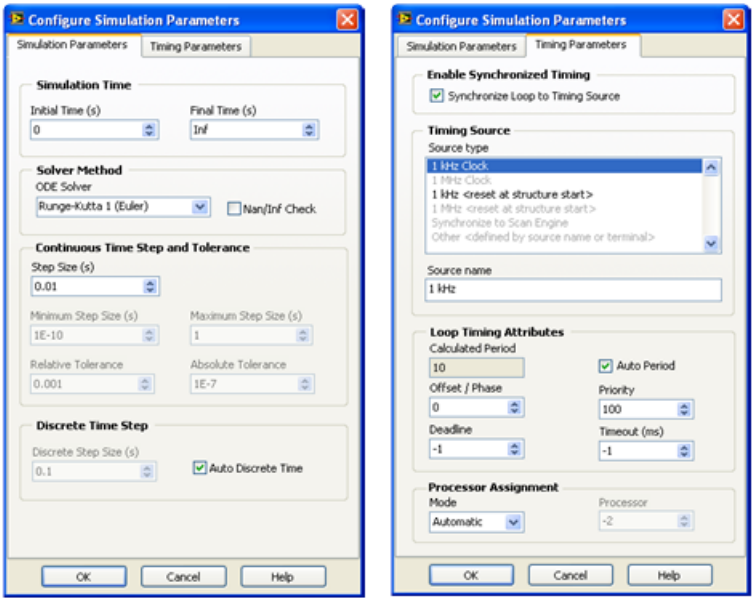

(a) **(b)**

Figure 1-7: Simulation Loop Parameters Dialog: (a) Simulation parameter (b) Timing Parameters

- Next, the QUBE-servo was configured to connect the myRIO by double click on HIL initialize block, and in the board, type filed MXP connector port was selected (e.g., qube_servo_myrio_mxp_a under Quanser Devices).
- Finally, the power LED on the QUBE-servo blinking, and the VI was started successfully without any errors.

B. Reading the Encoder

This step was started from the LabVIEW software in the control simulation loop. The encoder values of the motor at channale#0 were measured in pairs using the VI front panel in order to display the value of the motor position in degree, by following these steps:

- The HIL Read VI was added from Quanser Rapid Control Prototyping palette, as shown in Figure 1-12.
- The connection of the board out terminal from HIL Initialize to the board in terminal on HIL Read was established, as illustrated in Figure 1-13.
- Next, Double-click on HIL Read to configure the encoder input channel, and then set the Polymorphic Instance to Encoder (Scalar) to read signals from Encoder channel #0, as shown in Figure 1-14.
- The HIL Read can be scaled by multiplying the numeric indicator block by gain, as shown in Figure 1-12.
- Subsequently, the numeric value can be found in the front panel, as shown in previous Figure 1-10.

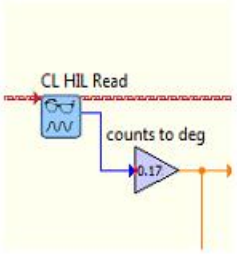

Figure 1-8.

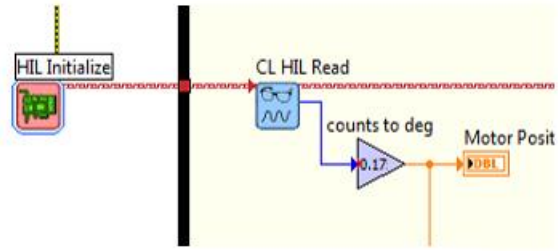

Figure 1-9.

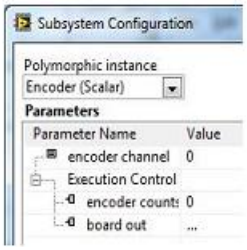

Figure 1-10.

- The online mode test was activated by starting the VI. As a result of this test, a number of counts on the numeric indicator was displayed which are proportional to the angle of the disk.
- The encoder reading start from zero for every time the VI is started, and even when the VI stop and restarted the numeric indicator shows a zero value because of the encoder poser lost its reference and always doesn't knows where it is positioned and that's why need to return to zero, which means that QUBE-servo DC motor embedded with incremental encoder.
- The counts of the encoder were measured for a full complete revolution where the disk set to zero position (0o degree), and then rotate the disk 360o degree. The result indicates that for one full rotation the encoder generates outputs of 2048 pules per one revolution.
- The count's pulses can be converted in degree by set the gain block to 0.175778125 (Gain $= \frac{\text{Degree}}{\text{No.of pulses}} = \frac{360^o}{2048} =$ 0.17578125)

C. Driving the DC Motor

This test indicated that the PWM operational amplifier operates the DC motor perfectly. The same procedure in the previous test was repeated with adding HIL Write block from Quanser Rapid Control Prototyping Toolkit palette, and then wire the board_out terminal HIL Read to the board in terminal on HIL Write as shown in Figure 1-15.

This block is used to drive the output from analog output channel#0 (AO0) as shown in the pin diagram of myRIO Figure 1-16. The numeric control was added to create the control by right-clicking on analog voltage terminal on HIL Write. Then, the constant and HIL Write analog blocks were also connected together. It is recommended as part of the procedure to use the abort button to terminate the simulation and added own stop button, as pictured in Figure 1-13. Also, auto-stop (HIL Stall Monitor) can be found in the same Figure 1-15 to protect the DC motor from damage as safety programming by observing the applied voltage and speed of the DC motor if a glitch may occur to the applied voltage of over 5V.

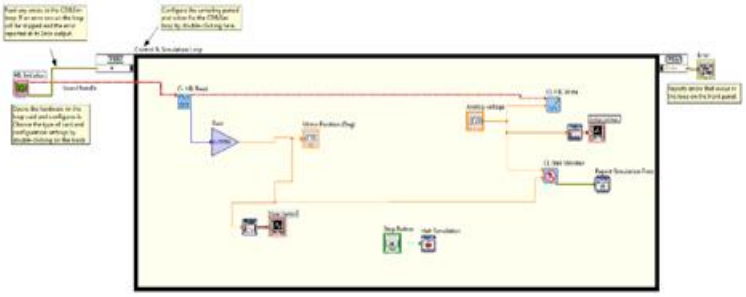

Figure 1-11.

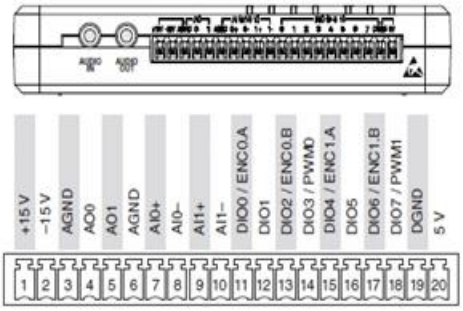

Figure 1-12.

- The simulation was tested by applying (0.5V) to drive the DC motor in the QUBE-servo (clockwise) which endorse that positive measurement was obtained when a positive signal is applied as shown in Figure 1-17. As the applied signal becomes negative (-0.5V) the disk was rotated reverse direction (counter-clockwise) as shown in Figure 1-18 which is important procedure assumption as stated in term of the design control system as measurement increasingly goes up with correlation to the angular speed of the DC motor in the QUBE-servo.

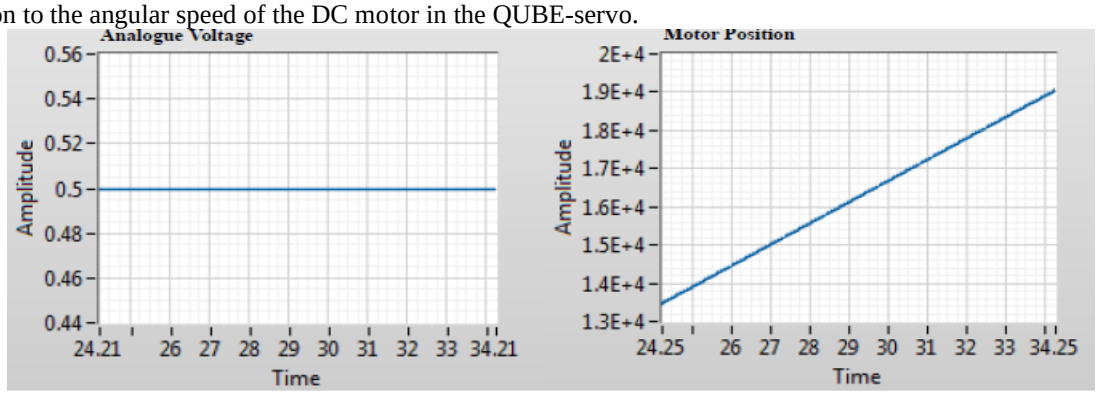

Figure 1-13: positive signal (0.5V) leads to rotate disk clockwise

D. Low Pass Filter implementation

- The VI model developed was taken to complete the next task, and where the encoder calibration gain was modified to measure the gear position in radians by a multiplied factor of $\frac{2\pi}{2048} = 0.003068$, as shown in Figure 1-19. Further to this step ,t he VI block diagram was programed with including the Inverse Modulus to define the range of the counter to reduce the discontinuous jump when counter memory filed reach the limit, and more functions should be taken into consideration in the VI coding area as advice in the manual student workbook.

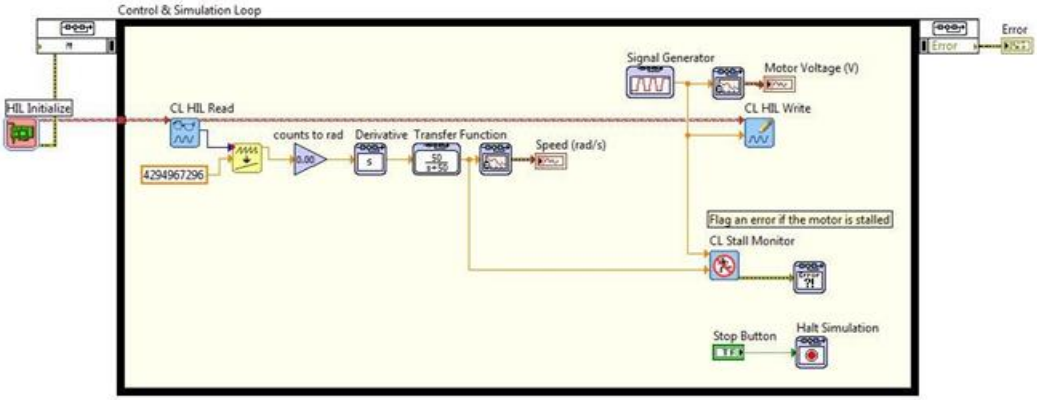

Figure 1-14: Measuring speed using encoder

Published By:
Blue Eyes Intelligence Engineering
and Sciences Publication (BEIESP)

- The VI shown in Figure 1-19 was built but without including the transfer function block. The range of valid readings confined in data acquisition counters size. So that to avoid discontinuous jump when encoder reaches the maximum range. The inverse modulus was added to block diagram as recommended in the user manual of the experiment. Moreover, the derivative block was added to the encoder calibration Gain output in order to measure the motor speed using the encoder (in rad/s).
- A signal generator can be found to drive the DC motor by applying continues square pulses voltage that goes from 1V to 3V at 0.4Hz in the parameters of a signal generator configuration, as shown in Figure 1-20.

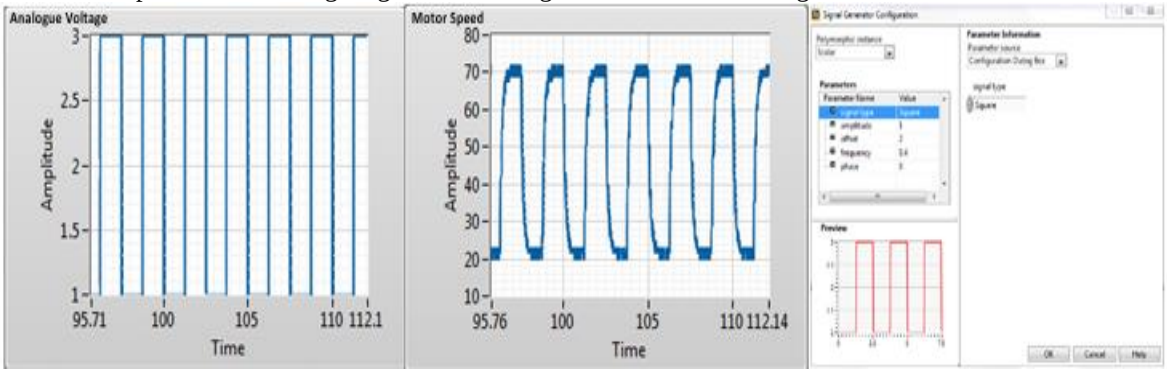

Figure 1-15: Measuring speed using encoder without applying low-pass filter, with parameters of signal generator configuration

- The VI was tested by running the simulation to measure the encoder position. A random signals noise was observed continuously over the measured period as shown in Figure 1-21. As such, the measured encoder angular speed is characterized as the rate of position corresponded to the time $\frac{d\theta}{dt}$ in digital forms, which define the key specification of digital sensors linearity tolerance that meanly depends on length of the track of code disk and the gap length of the black lines and transparent lines where the beam pass through to generate the discrete signal as illustrated in Figure 1-6. The greater gap of code disk and transparent lines, the lower accuracy that can be achieved in terms of resolution. The variation in the linearity of the position response of the encoder can be found in the section as shown in Figure 1-22 which means that position response has a discontinuous (discrete) signal because of the slope of the of $\frac{d\theta}{dt}$ has an incremental variation in angular position [14].

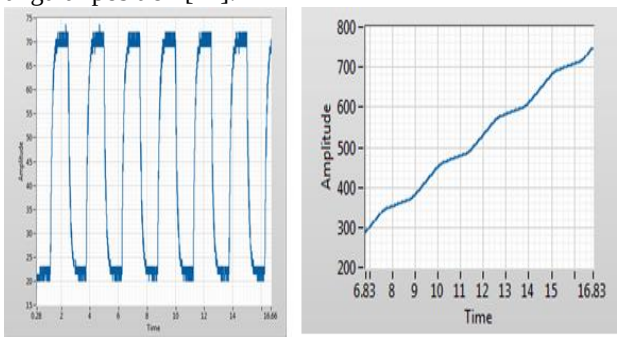

Figure 1-16: Motor speed (with noise) Figure 1-17:

Encoder position

- The transfer function block which demonstrating the low-pass filter was added after the derivative output block and connected the low-pass filter to the scope. The low-pass transfer function set to $G(s) = \frac{50}{s+50}$, as illustrated in Figure 1-19. The VI simulation was examined where a positive result was observed to reduce the effect of the noise on the output response as shown in Figure 1-23.

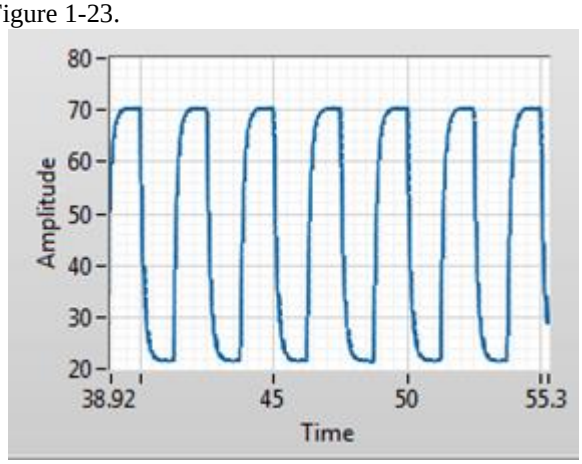

Figure 1-17: Motor speed (reduced noise)

- The cutoff frequency of the low-pass filter can be found $\omega_f = 50$ rad/s and $f_f = \frac{50}{2\pi} = 7.96$ Hz
- Finally, the cutoff frequency was varied ω_f between 10 to 200 rad/s. As for the first order low pass filter, the higher frequency components will be difficult to pass and attenuated to at least −3dB ≈ 50%.

Hence, the cutoff frequency is the ratio of the $\frac{Vo}{Vi}$ that has a magnitude of $\frac{1}{\sqrt{2}}$. This magnitude can be converted to 3dB using the following equation ➔ Magnitude = $20\log_{10}\left(\frac{Vo}{Vi}\right)$, where at this point the cutoff frequency increased the amount of attenuation as the frequency cumulative as shown in Figure 1-24,25&26.

Published By:
Blue Eyes Intelligence Engineering
and Sciences Publication (BEIESP)

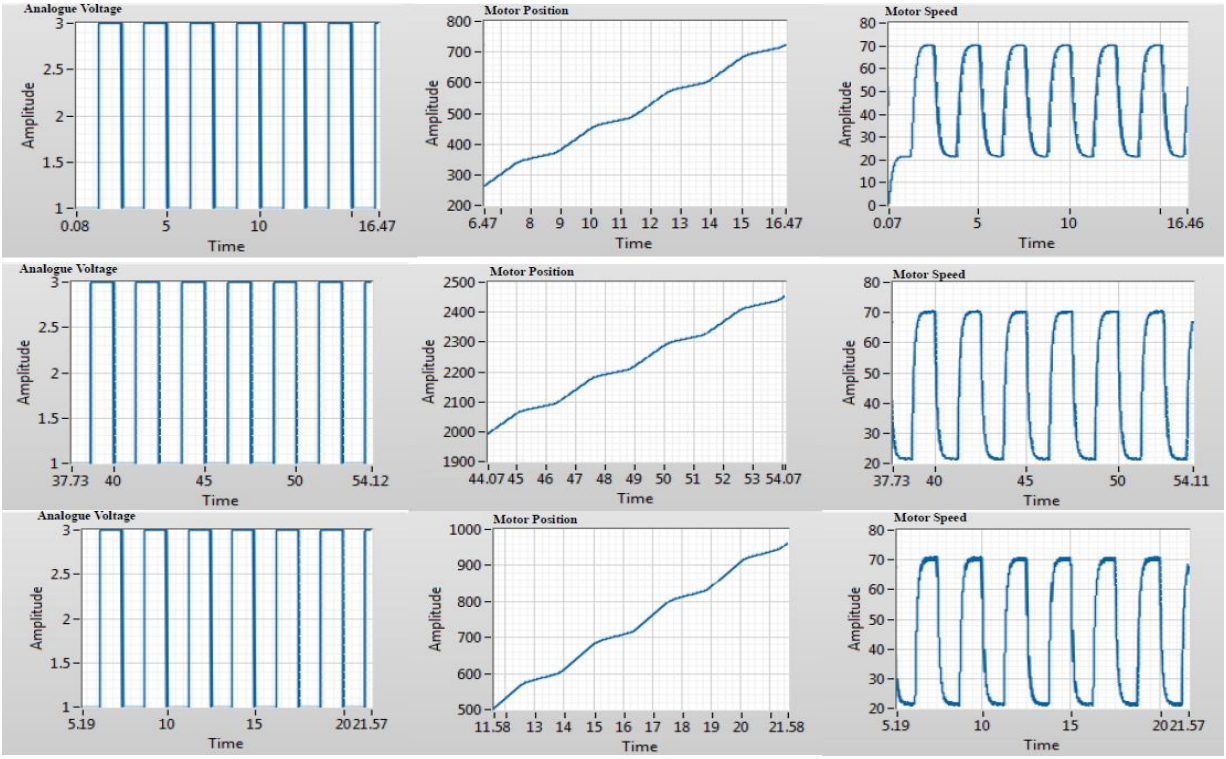

Figure 1-18: $\omega_f = 200\ rad/s$

The cutoff frequency is equal $\omega_f = \frac{1}{\tau}$, where τ is the time constant. The relation between cutoff frequency and the time constant comes from the following:

$$G(s = j\omega) = \frac{\frac{1}{\tau}}{s + \frac{1}{\tau}} = \frac{1}{j\omega * \tau + 1}$$

$$|G(s = j\omega)| = |\frac{1}{j\omega * \tau + 1}|$$

$$Magnitude = \sqrt{\frac{1}{\omega_f^2 \tau^2 + 1}}$$

Where the magnitude $= \frac{1}{\sqrt{2}} \rightarrow \sqrt{\frac{1}{\omega_f^2 \tau^2 + 1}} = \frac{1}{\sqrt{2}}$, *by solving for*

$\omega_f = \frac{1}{\tau}$

So, since the relation between the cutoff frequency and time constant is revers relation. This means that as the frequency increase the time constant decrease, as calculated in the following table 1-4:

ω_f	*10 rad/s*	*20 rad/s*	*50 rad/s*	*100 rad/s*	*150 rad/s*	*200 rad/s*
τ	*0.1 s*	*0.05 s*	*0.02 s*	*0.01 s*	*0.006 s*	*0.005 s*

E. Stability analysis

The VI was configured based on the design in previous steps with applied a step of 1 V to the DC motor and measuring the servo speed and the position from encoder signal, as pictured in Figure 1-27.

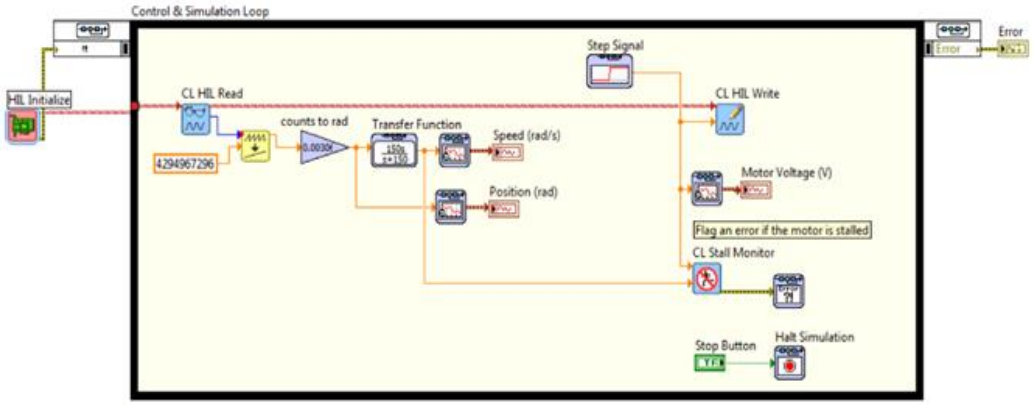

Figure 1-19: Measuring speed and position when applying a step

- The stability of the system of the voltage to speed was determined based on the poles of the transfer function $\frac{\Omega_m(s)}{v_m(s)}$ ➔ $s + \frac{1}{\tau}$ ➔ $s = -\frac{1}{\tau} = \frac{1}{0.13} = -7.6923$, which means system is stable.
- In this part, the stability of the voltage to position also determined by identifying the poles from the transfer function $\frac{\Theta_m(s)}{v_m(s)}$ ➔ $s(s + \frac{1}{\tau})$ ➔ $s = 0$, and $s = -\frac{1}{\tau} = \frac{1}{0.13} = -7.6923$, which means system is marginally (critically) stable.
- The unit step voltage was applied by running the simulation VI, and also the simulation loop configured to be run for 2.5 sec. The following results response were observed as shown in Figure 1-28:

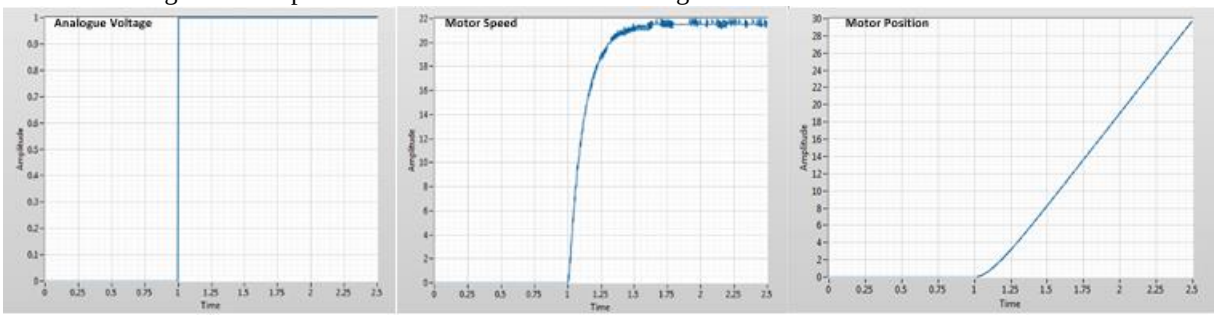

Figure 1-20: Measuring speed and position when applying a unit step

The output result was compared with step response in workbook manual (Figure 10) which is similar to motor position and speed response.

- The stability was checked based on the conditions rule of the BIBO stability principle. The motor speed of the above Figure 1-29 is stable for bounded input yields to a bounded output (BIBO). As for the motor position, the output response is unstable for bounded input yields an unbounded output (BIUBO). Moreover, the principle of BIBO approach was compared with the results from the poles analysis as follow table 1-5:-

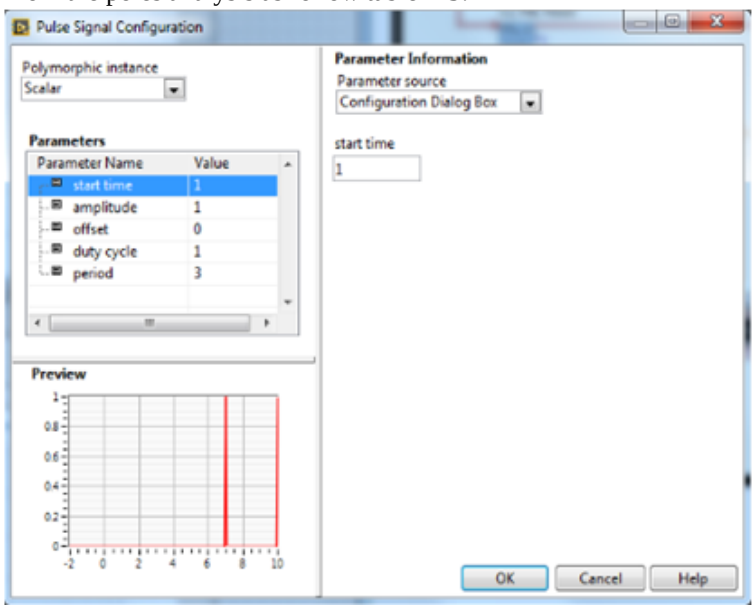

Figure 1-21: Pulse signal configuration

Function	Pole analysis	BIBO
Motor speed $\frac{\Omega_m(s)}{v_m(s)}$	stable	stable
Motor position $\frac{\Theta_m(s)}{v_m(s)}$	marginally stable	unstable

- The input response was modified as pictured in Figure 1-30. The impulse response was used to run the simulation VI. Based on the following results Figure 1-28, the system can be found to be stable because of the short pulse applied for a short period will eventually lead to stable position in term of bounded inputs. Then, the sinusoidal response was applied to the input analog voltage, hence a continuous oscillation was observed within the time period which means that the system is unstable in term of bounded inputs as shown in Figure 1-31.

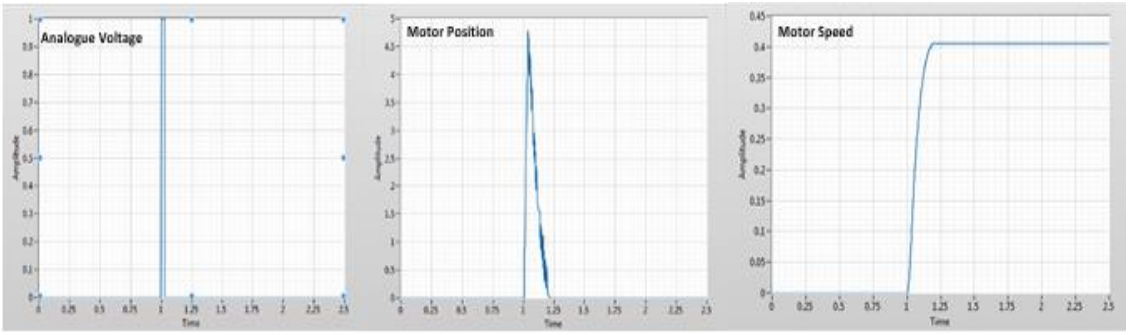

Figure 1-22: Results of output response of analogue voltage, motor speed, and motor position when applied step input

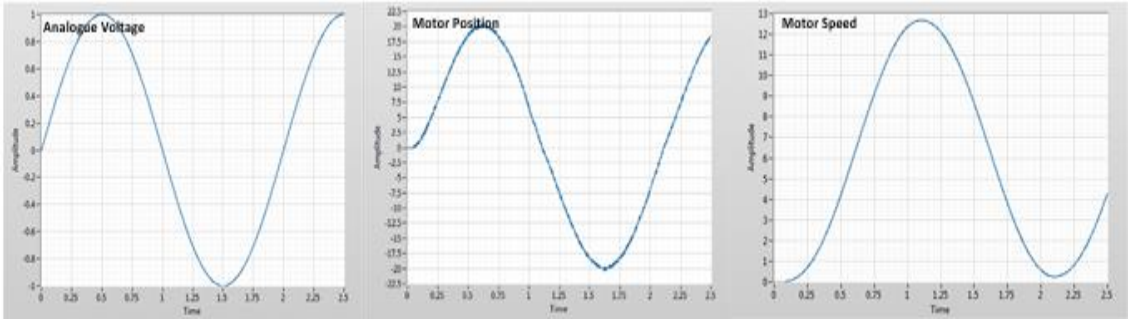

Figure 1-23: Results of output response of analogue voltage, motor speed, and motor position when applied sinusoidal input

III. CONCLUSION

In this report, a deep investigation has been carried out to understand the concept of data servo system and data acquisition in terms of the working principle both in hardware and software by enhancing the hands-on skill and applying different mode tests such as creating a LabVIEW virtual interface VI, drive DC motor, read encoder signal, low pass filter, and stability analysis. The results obtained in this experiment were confirmed that a servo system and information monitoring using data acquisition controller have proportional relation in term of angular velocity and shaft position of the DC motor. The transfer function model of the DC motor in the QUBE-servo has driven analytically, and its parameters are evaluated to understand system behavior. The filtering block used to eliminate the high-frequency components of a signal has a model of the first-order low pass in the form of transfer function wherein examined with different frequency ranges. In addition, the QUBE-servo was modeled and simulated using base time software with examined different parameters as stated in the experiment workbook. Further study has been conducted stability analysis for two types of approach BIBO and poles analysis. Both approaches have similar to determine the stability of the system. The step input, impulse and sinusoidal can be found in this report to study the cornerstone of the system. From the simulation result, this report confirms that the step size of the system which defines the sampling time has an inverse relationship in terms of resolution and information collected to represent the responses. A further study to the sensitivity of the system that could help to understand deeply the long-term effects of noise and how to eliminate them.

REFERENCES

1. I. Boldea, "Electric generators and motors: An overview," CES Transactions on Electrical Machines and Systems, vol. 1, no. 1, pp. 3-14, 2017.
2. M. Yildirim, M. Polat, and H. Kürüm, "A survey on comparison of electric motor types and drives used for electric vehicles," presented at the 2014 16th International Power Electronics and Motion Control Conference and Exposition, Antalya, Turkey, 2014.
3. A. S. Sadun, J. Jalani, and J. A. Sukor, "A Comparative Study on the Position Control Method of DC Servo Motor with Position Feedback by using Arduino," ARPN Journal of Engineering and Applied Sciences, vol. 11, no. 18, pp. 10954–10958, 2016.
4. N. Pinckney, "Pulse-width Modulation for Microcontroller Servo Control," IEEE Potentials, vol. 25, no. 1, pp. 27-29, 2006.
5. Quanser. (2019). QUBE - Servo 2 - Quanser. Available: https://www.quanser.com/products/qube-servo-2/
6. R. C. Dorf and R. H. Bishop, Modern Control Systems 2010,ISBN-13:978-0-13-602458-3
7. M. Afandi, H. Adinanta, A. Setiono, B. Qomaruddin, and Widiyatmoko., "High resolution extensometer based on optical encoder for measurement of small landslide displacements," presented at the Journal of Physics: Conference Series, 2018.
8. H. V. Hoang and J. W. Jeon, "An Efficient Approach to Correct the Signals and Generate High-Resolution Quadrature Pulses for Magnetic Encoders," IEEE Transactions on Industrial Electronics, vol. 58, no. 8, pp. 3634-3646, 2011.
9. G. Liu, S. Chen, S. Zheng, and X. Song, "Sensorless Low-Current Start-Up Strategy of 100-kW BLDC Motor With Small Inductance," IEEE Transactions on Industrial Informatics, vol. 13, no. 3, pp. 1131-1140, 2017.
10. N. Li Ying and Ertugrul., " A novel, robust DSP-based indirect rotor position estimation for permanent magnet AC motors without rotor saliency," IEEE Transactions on Power Electronics, vol. 18, no. 2, pp. 539–546, 2003.
11. H. Zumbahlen, Linear Circuit Design Handbook. Amsterdam: Boston: Elsevier/Newnes Press., 2008.
12. S. Chen, G. Liu, and S. Zheng, "Sensorless Control of BLDCM Drive for a High-Speed Maglev Blower Using Low-Pass Filter," IEEE Transactions on Power Electronics vol. 32, no. 11, pp. 8845–8856., 2017.
13. A. Soltan, G. Radwan, and M. Soliman, "Fractional Order Sallen–Key and KHN Filters: Stability and Poles Allocation," Circuits, Systems, and Signal Processing, vol. 34, no. 5, pp. 1461-1480, 2015.
14. M. Ponmalar et al., "Demonstration of High Resolution Absolute Optical Encoder by Piecewise Linear Approximation.," 2018 IEEE SENSORS, vol. 2018, pp. 1-3, 2018.

AUTHOR PROFILE

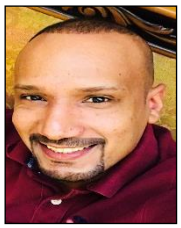

Khaled S AlRasheed, (B.Sc.Eng 1998-MS 2010, PHD 20221), is currently an Senior specialized engineer at Public Authority for Applied Education and Training-Higher Institute of Energy(HIE)-Electrical Power Department (PAAET). He received B. Eng. (V Good) in Electrical and Electronics Engineering from New Mexico State University (USA), and later received MSc from University of Mansour Egypt in Electrical Engineering. He was later Leadership at HIE-Students Affairs (2012-2016), then a Leadership at HIE-Training Committee, and Adviser in the scientific club in Kuwait (Since 2008). PHD in Islamic International University of Malaysia. Interest in Renewable Energy (solar), Power Electronics.

Muhammad R A A Jamal, B. Sc. in Electrical Engineering, M.Sc. in Embedded Systems and Instrumentations. Spent 6 years in the instrumentation and control engineering at Doha Power Station, Kuwait. Currently member of training staff in the Higher Institute of Energy PAAET, Kuwait, since 2008. Dedicated in industrial automation and sensors. Worked as embedded system consultant in prototypes development.

Meshari J AlJandal, (B.Sc.Eng 2005-MS 2019), is currently a specialized engineer at Public Authority for Applied Education and Training-Higher Institute of Energy(HIE)-Electrical Power Department (PAAET). He received B. Eng. (V Good) in Electrical Engineering from Kuwait University, and later received MSc from University of Newcastle upon Tyne in Automation and control. He was working as maintenance engineer at wire cable manufacturing (2005-08), then promoted as senior production engineer (2008-2010), then a Leadership at product development firm Worked as consultant in prototypes development (since 2015).